Supporting Information

Table S1. **Consistency of the GMMA-4 data set of Figure 1, consisting of SPR-SC, ITC, SV-AUC, and FP.** Pair-wise consistency matrix $C_{ef} = \chi^2_e{}^{(\text{fit } e,f)}/\chi^2_e{}^{(\text{fit } e)}$ (Eq. 1), related to a confidence level by F-statistics. Reported is the value of *P* at which the differences in quality of fit could arise by chance and the sets could be considered consistent; by this measure, high ratios C_{ef} require large *P*-values. Similarly, C_e^* measures the decrease in the quality of fit of all other data sets except *e* caused by including *e* into the GMMA.

e	C_e* all others	C_{ef} SPR-SC	C_{ef} ITC	C_{ef} SV-AUC	C_{ef} fluorescence anisotropy
SPR-SC	0.30	-	0.079	0.24	0.0035
ITC	0.66	0.52	-	0.13	0.0040
SV-AUC	0.35	0.059	0.060	-	0.0050
fluorescence anisotropy	1.5×10^{-6}	0.10	0.43	0.19	-

Table S2. **Values of the information matrix I_{ep} for the GMMA-4 data set.** The values of I_{ep} describe the factor increase in the error estimate of parameter *p* when the experiment *e* is left out of the global analysis. The error estimates are based on the diagonal entries of the covariance matrix.

e	SPR-SC	ITC	SV-AUC	fluorescence anisotropy
$\log_{10}(K_1)$	2.59	1.003	1.066	1.038
$\log_{10}(K_2 / K_1)$	2.23	1.11	1.22	1.025
ΔH_1	1.23	∞	1.002	1.004
$\Delta H_2 - \Delta H_1$	1.21	∞	1.011	1.003
s_{11}	1.070	1.15	∞	1.001
s_{21}	1.0011	1.18	∞	1.0002

<u>Figure S1.</u> GMMA fit including direct SPR surface binding isotherm, in addition to SPR-SC, ITC, SV-AUC, and FP from Figure 1. Data are shown in the same representation as Figure 1, with the addition of SPR direct surface binding data in Panel (a) (triangles). The new GMMA best fit curves are shown in red.

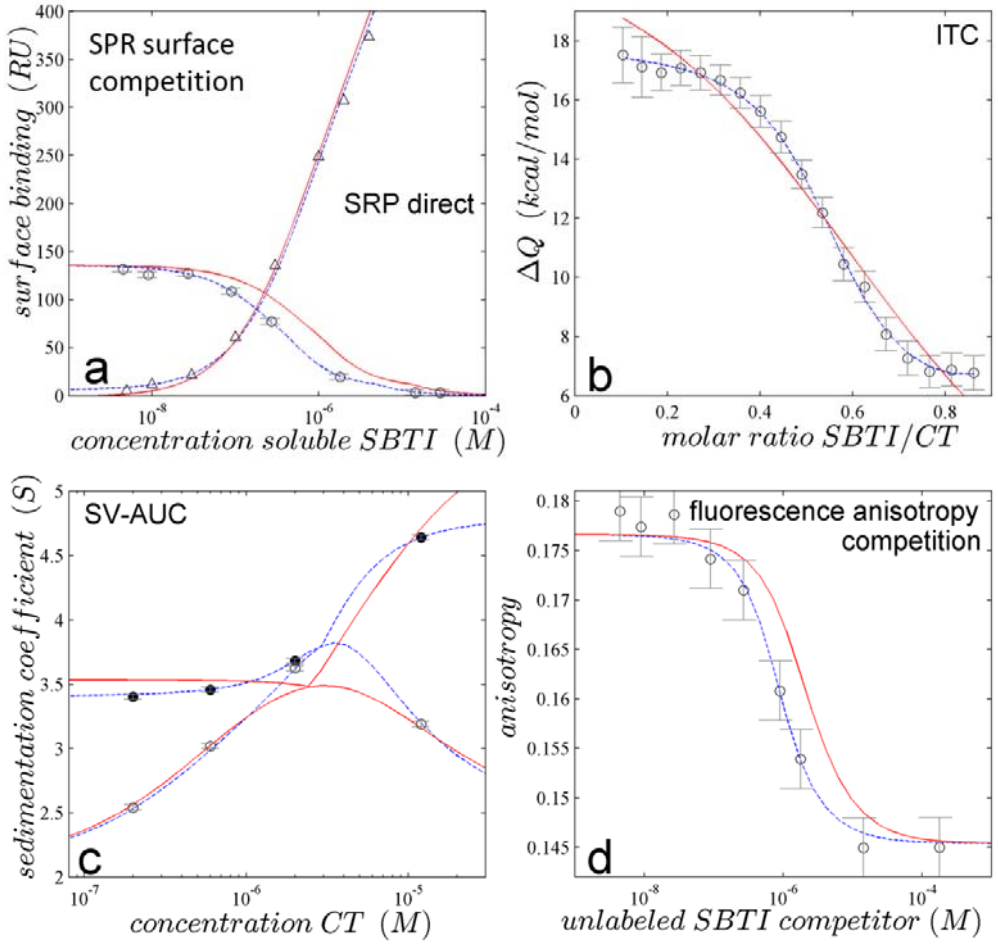

Table S3. **Consistency matrix of the GMMA data from Figure S1.** Pair-wise consistency matrix $C_{ef} = \chi^2_e{}^{(\text{fit } e,f)}/\chi^2_e{}^{(\text{fit } e)}$ (Eq. 1), related to a confidence level by F-statistics. Reported is the value of *P* at which the differences in quality of fit could arise by chance and the sets could be considered consistent; by this measure, high ratios C_{ef} require large *P*-values. Similarly, C_e^* measures the decrease in the quality of fit of all other data sets except *e* caused by including *e* into the GMMA.

e	C_e* all others	C_{ef} SPR direct	C_{ef} SPR-SC	C_{ef} ITC	C_{ef} SV-AUC	C_{ef} fluorescence anisotropy
SPR direct	**(1-P) < 10^{-6}**	-	0.18	0.96	0.15	1.4×10^{-4}
SPR-SC	0.008	**1.0 - 4×10^{-4}**	-	0.079	0.24	0.0034
ITC	0.060	**(1-P) < 10^{-6}**	0.48	-	0.095	0.36
SV-AUC	0.027	**1.0 - 5×10^{-3}**	0.059	0.059	-	0.0050
fluorescence anisotropy	4.0×10^{-11}	**1.0 - 1×10^{-3}**	0.11	0.41	0.18	-

Values in bold show that SPR direct surface binding data are highly inconsistent with all the others.

Figure S2. Global single-method analysis of four ITC titrations 'multi-4 ITC'

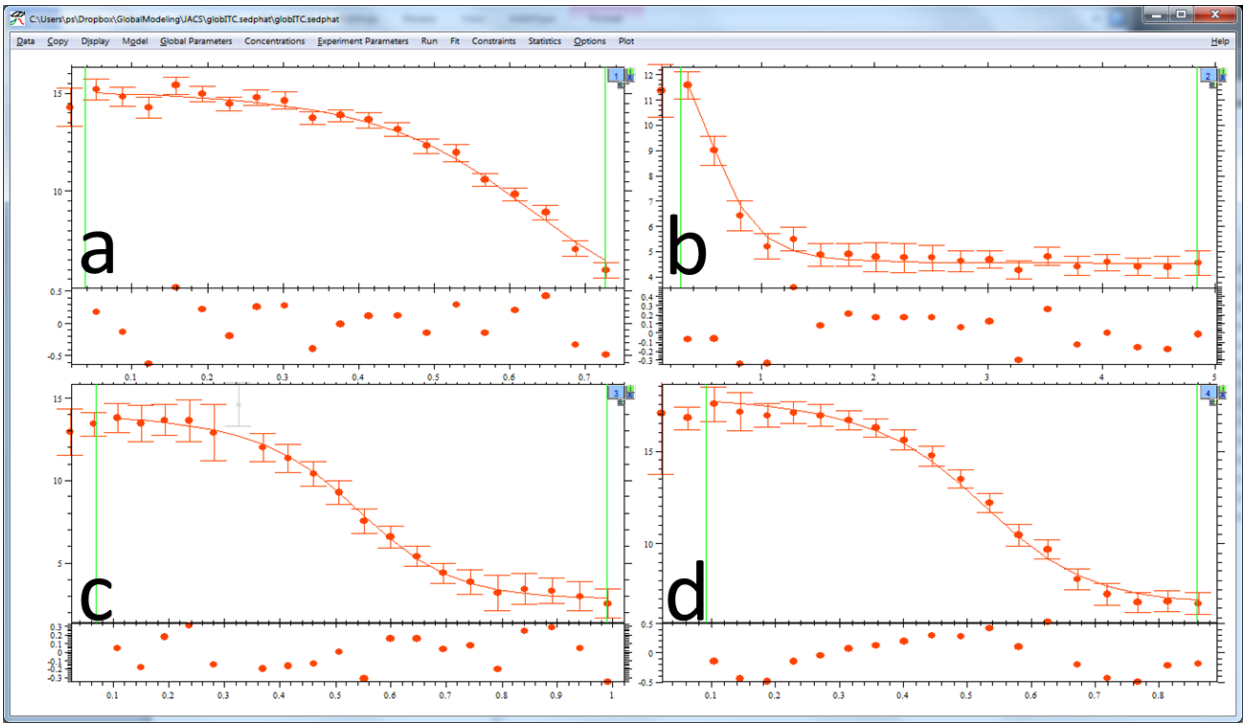

SEDPHAT screenshot of the global ITC fit. For each experiment a pair of two panels is shown, the larger one showing the isotherm data (symbols) and best-fit model (solid lines), and the smaller one showing the residuals of the fit (symbols). Best-fit parameters and error estimates as presented in Figure 2, blue bars. Conditions for each experiment are

(a) 68.4 µM SBTI titrated in 22.7 µM CT. In this experiment only, due to an error in the concentration of CT a correction factor for the cell concentration was introduced as local, adjustable parameter (similar to the conventional 'n-value' in ITC analysis).
(b) 68.4 µM SBTI titrated in 3 µM CT.
(c) 83.7 uM SBTI titrated in 20 µM CT.
(d) 83.7 uM SBTI titrated in 20 µM CT, also part of 'GMMA 4' and shown in Figure 1.

ITC experiments (a) and (b) were conducted originally as preliminary experiments to explore useful concentration ranges and titration schedules for 'optimal' experiments. Even though these data sets (a) and (b) individually do not permit observation of the full titration range, their inclusion into the global data set greatly increases the information content of the ITC data, as can be discerned in Figure 2 from the reduced parameter uncertainties of 'multi-4 ITC' compared to 'ITC only'.

Figure S3. Screenshot of the extended GMMA fit 'GMMA-9'

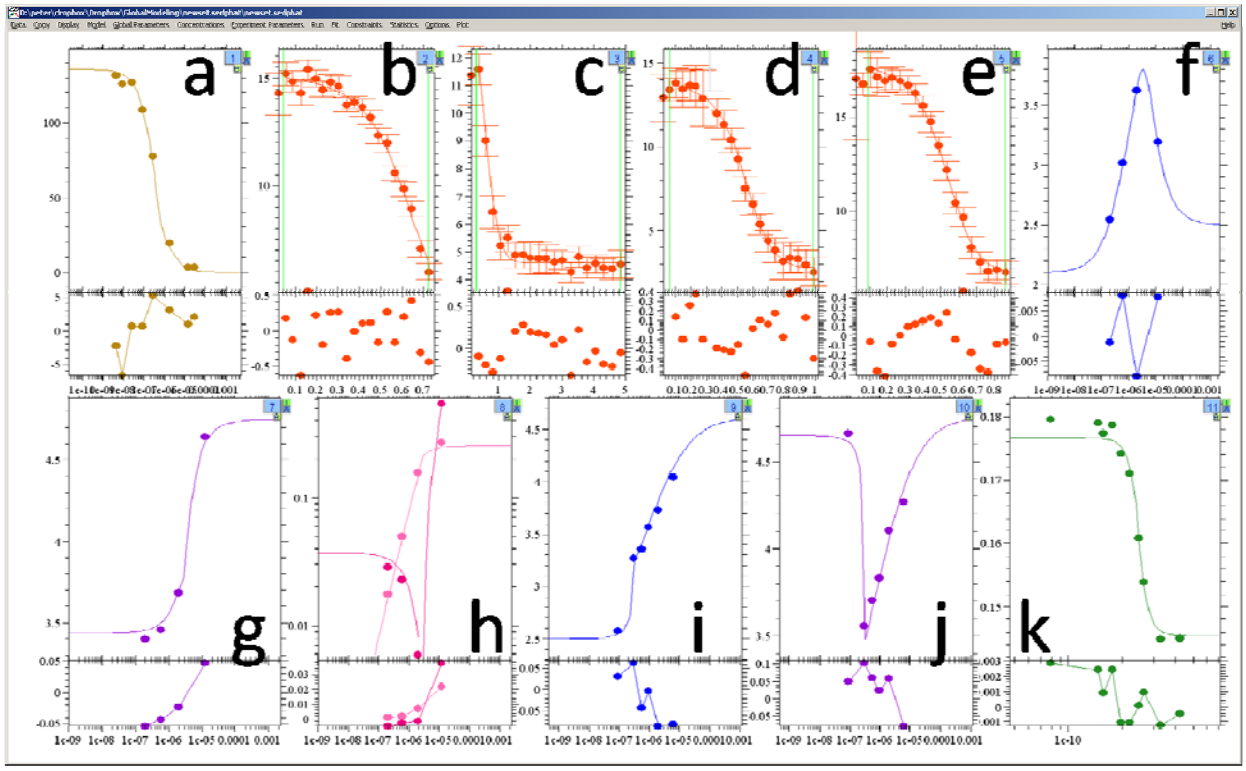

For each experiment a pair of two panels is shown, the larger one showing the isotherm data (symbols) and best-fit model (solid lines), and the smaller one showing the residuals of the fit (symbols). Best-fit parameters and error estimates as presented in Figure 2, red bars. The multi-method data set is comprised of

(a) SPR-SC experiment, also part of 'GMMA 4' and shown in Figure 1.

(b-e) ITC experiments as specified in Figure S2, where (e) is also part of 'GMMA-4' shown in Figure 1.

(f-h) SV-AUC titration series of 1.8 µM SBTI with 0.2 – 12 µM CT, producing two data sets with weighted average sedimentation coefficient (f) and s-value of the reaction boundary (g). These data are also part of 'GMMA 4' and shown in Figure 1. From the same titration series, (h) are the boundary amplitudes.

(i-j) SV-AUC dilution series of 0.3 – 6 µM SBTI with 2.1-fold excess of CT, combined with a first isotherm point from an experiment with 0.09 µM SBTI and 10 µM CT. This series produced two data sets with weighted average sedimentation coefficient (i) and s-value of the reaction boundary (j) . (The solid line in this case is based on a trajectory that is curved in concentration parameter space.)

(k) Fluorescence anisotropy titration experiment (k) of 0.09 µM Dylight488-labeled SBTI and 1 µM CT with 0.0045 – 179.90 µM unlabeled SBTI, also part of 'GMMA 4' and shown in Figure 1.

Figure S3. GMMA of the 4 ITC titrations combined with SPR-SC

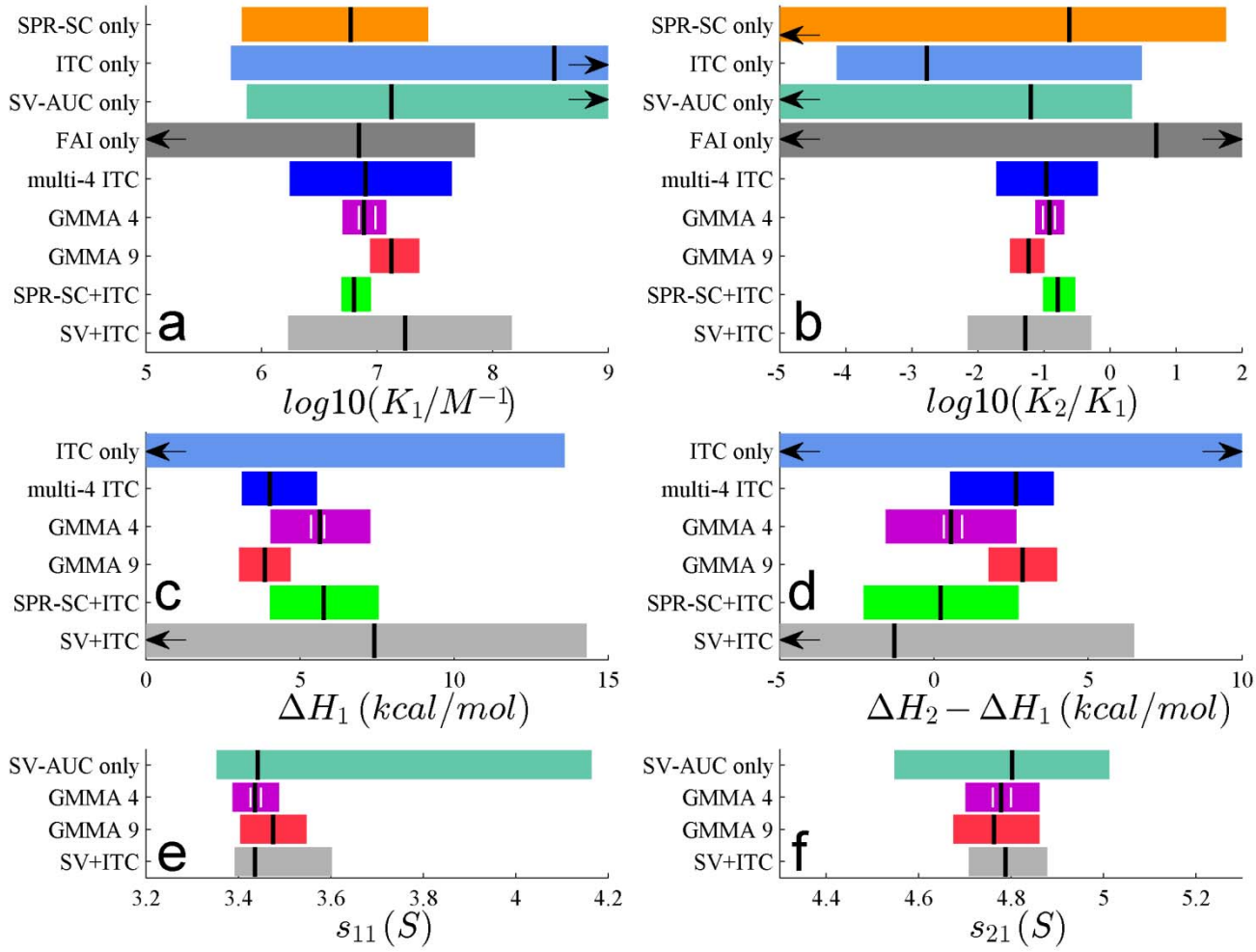

Analogous to Figure 2, shown are best-fit parameter estimates (vertical black lines) and 68% confidence intervals (colored bars) from different analyses. For comparison, the data from Figure 2 are repeated, with additional data: 'SPR-SC+ITC' (light green) from the GMMA of the combination of SPR-SC with a single ITC data set (combining the data from Figure 1a and 1b); and 'SV+ITC' (light grey) from the GMMA of the combination of SV-AUC with a single ITC data set (combining the data from Figure 1b and 1c).

Auxilliary Computational Methods: Detailed fitting functions for each method

Surface plasmon resonance surface binding and surface competition

In SPR surface binding, for a simple 1:1 binding model of two proteins with equilibrium dissociation constant K_D, the steady-state binding signal of an analyte A in a flow across the sensor surface with the immobilized binding partner B_S ideally follows the Langmuir isotherm

$$f_{e,i} = \frac{R_{\max,e}}{1 + c_{A,i} / K_D} + b_e \qquad \text{(Eq. S1)}$$

where $R_{max,e}$ denotes the maximum surface binding capacity and b_e denotes a baseline offset, both local parameters, and $c_{A,i}$ denotes the molar analyte concentration for data point i [1].

In case the surface attachment causes artifacts, such as alterations in the binding affinity or the creation of multiple subpopulations with different affinities, the steady-state surface binding signal (or any other reproducible feature of the binding progress curve) as a function of analyte concentration $R(c_A)$ may be sampled at a range of analyte concentrations and interpolated to represent an empirical calibration of the sensor signal. We then can conduct a competition binding experiment with mixtures of soluble analyte A, a soluble form of the immobilized partner B and potentially other components C, D, etc. Assuming that only soluble A interacts with the surface sites, the binding data can then be modeled as

$$f_{e,i} = R\left(c_A\left\{c_{Xtot,i}\right\}\right) \qquad \text{(Eq. S2)}$$

where the free analyte concentration of A in the mixture flowing across the sensor surface is a function of solution composition and calculated on the basis of mass action law. In this form, strictly the solution interaction is probed, independent of surface artifacts, and there are no local adjustable parameters. It is not necessary to make the assumption that the surface binding follows a Langmuir isotherm.

The mass action law in Eq. S2 can expressed generally as

$$c_{Xtot}\alpha_X = c_{X,free} + \sum_{\kappa} \nu_{\kappa,X} K_\kappa \prod_{X'} c_{X',free}^{\nu_{\kappa,X}} \qquad \text{(Eq. S3)}$$

, linking the free and total molar concentrations of all components X forming complexes κ with stoichiometry $\nu_{\kappa,X}$ and affinity constants K_κ. The factor α_X in this equation accounts for a concentration error of component X.

Isothermal titration calorimetry

Modeling ITC data follows the approach outlined previously [2]. In brief, the changes in heat measured upon changing the solution composition are generally described as

$$f_{e,i} = \Delta Q_i + b_e = \sum_{\kappa} \Delta H_{\kappa} \left(c_{\kappa} \left(\left\{ c_{Xtot,i} \right\} \right) - c_{\kappa} \left(\left\{ c_{Xtot,i-1} \right\} \right) \right) - \sum_{\kappa} \Delta H_{\kappa} \frac{\Delta V_i}{V_0} c_{\kappa} \left(\left\{ c_{Xtot}^{(syringe)} \right\} \right) + b_e$$

(Eq. S4)

where ΔH_{κ} denotes the enthalpy change from formation of complex κ, and $c_{\kappa}\{c_{Xtot,i}\}$ reflects the cell concentration of complex κ, after accounting for dilution effects, after titration step *i*, calculated after Eq. S3. The second term allows for heats from the dissociation of pre-formed complexes in the syringe. The traditional '*n*-value' used to describe compounded concentration errors are not compatible with global modeling [2], and instead the factors α_X, or equivalently incompetent fractions, account for the commonly observed errors in the active component concentrations. Dependent on whether the same error α_X can be expected in different experiments or not, α_X can be a local parameter for only one experiment or be shared among multiple ITC experiments. For the data in the present study, unless otherwise mentioned the factor α_X was fixed at a value of 1.0.

Sedimentation velocity analytical ultracentrifugation

As outlined in [3,4], in principle, families of raw data scans reporting the signal as a function of radial position and time can be modeled in SEDPHAT directly with Lamm partial differential equation solutions for the coupled reaction/diffusion/sedimentation process (Lamm PDE). Multiple of such data sets acquired at different wavelengths and with different optical systems, at different rotor speeds, and at different loading composition can be included in GMMA. In this case, in addition to the global parameters of sedimentation coefficients and buoyant molar masses of each species (some of which can be constrained), local parameters representing the meniscus and bottom position of the solution column, as well as time time-invariant and radial-invariant noise components arise.

The utility of such direct Lamm PDE modeling is limited to cases where highly mono-disperse material for each component is available. More robust and tolerant to sample impurities is a hierarchical approach that consists in the direct modeling of the SV-AUC data first with sedimentation coefficient distributions *c(s)*, followed in a second step by integration to extract the salient data describing the amplitudes and velocities of the boundary pattern formed at different loading concentrations [5]. For example, isotherms of weighted average sedimentation coefficients can be modeled with general expressions

$$f_{e,i} = s_w(\{c_{Xtot,i}\}) = \frac{\sum_X \varepsilon_{\lambda,X} c_{X,free,i} s_{X,free} + \sum_\kappa \left(\sum_X \nu_{\kappa,X} \varepsilon_{\lambda,X} \right) c_\kappa(\{c_{Xtot,i}\}) s_\kappa}{\sum_X \varepsilon_{\lambda,X} c_{Xtot}} \qquad \text{(Eq. S5)}$$

where $c_\kappa(\{c_{Xtot,i}\})$ is the concentration of each complex species at each experimental mixture *i*, calculated on the basis of mass action law Eq. S3, $\varepsilon_{\lambda,X}$ denotes the extinction (or signal) coefficient of component *X*, assuming no hyper- or hypo-chromicity, and $s_{X,free}$ and s_κ are the sedimentation coefficients of the free and complex species, respectively [6]. The sedimentation coefficients reflect the hydrodynamic shape of the species and are global parameters, whereas extinction and signal coefficients are local parameters, which may be shared. (The extinction coefficients are dependent on the quality of the spectrophotometer used, and therefore can usually not be treated as global parameters.) A term multiplicative to Eq. S5 can be added to account in a first approximation for hydrodynamic interaction as a function of the total weight concentration of macrosolutes, adding the non-ideality coefficient k_S as a global parameter [7,8].

Similarly, the sedimentation velocity of the reaction boundary, as well as the amplitudes of the undisturbed boundary and the reaction boundary, can be modeled with simple analytical expressions on the basis of the effective particle theory [5,9]. For example, for a molecule B with n sites for A, the sedimentation coefficient of the reaction boundary

$$f_{e,i} = s_{fast}(\{c_{Xtot,i}\}) = \begin{cases} \left(s_A c_{Afree,i} + \sum_{j=1}^{n} j s_{AjB} c_{AjB,i} \right) \Big/ \left(c_{Afree,i} + \sum_{i=1}^{n} j c_{AjB,i} \right) & c_{Bfree,i} > c_B^*(c_A) \\ \left(s_B c_{Bfree,i} + \sum_{j=1}^{n} s_{AjB} c_{AjB,i} \right) \Big/ \left(c_{Bfree,i} + \sum_{j=1}^{n} c_{AjB,i} \right) & else \end{cases}$$

(Eq. S6)

with c_B^* the critical concentrations of free B for the phase transition of the boundary pattern [9], s_{AjB} and c_{AjB} denoting the complex species sedimentation coefficients and concentrations, and where all species concentrations are determined by mass action law Eq. S3.

Sedimentation equilibrium analytical ultracentrifugation

The models for SE-AUC are based on well-known Boltzmann exponentials for the radial distribution of species in chemical equilibrium and ideal sedimentation equilibrium [10,11]. In brief,

$$f_{e.i} = \sum_X d\varepsilon_{\lambda,X} c_{X,free}(r_0) e^{M_{b,X} H (r_i^2 - r_0^2)} + \sum_\kappa d\left(\sum_X \nu_{\kappa,X} \varepsilon_{\lambda,X} \right) c_\kappa(r_0) e^{\left(\sum_X \nu_{\kappa,X} M_{b,X} \right) H (r_i^2 - r_0^2)} + b_e(r)$$

(Eq. S7)

with the abbreviation $H = \omega^2 / 2RT$, the optical pathlength *d*, and the buoyant molar masses of all components $M_{b,X}$. The species concentrations at the reference radii, $c_\kappa(r_0)$, are related to the free species concentrations $c_{Xfree}(r_0)$ by mass action law. $c_{Xfree}(r_0)$ are either treated as new local parameters, or, preferably, calculated on the basis of total loading concentrations $\{c_{Xtot,i}\}$ with implicit mass conservation constraints between different data sets from the same cell at multiple rotor speeds. The latter requires the radial position of the end of the solution column to be treated as a local (shared) parameter, and offers the opportunity to allow radial-dependent baselines as local (shared) parameters. More detailed reviews of this approach can be found in [10–12].

Fluorescence and other linear spectroscopy

Spectroscopy data models in SEDPHAT are based on a linear superposition of signals of each species, requiring the absence of inner filter effects or other sources of non-linear signals. Briefly, the total signal or count-rate as a function of solution composition is expressed as

$$f_{e.i} = \sum_X \varepsilon_{\lambda,X} c_{X,free,i} + \sum_\kappa \left(\Delta\varepsilon_{\lambda,\kappa} + \sum_X \nu_{\kappa,X} \varepsilon_{\lambda,X} \right) c_\kappa(\{c_{Xtot,i}\}) s_\kappa \qquad \text{(Eq. S8)}$$

, where the binding signal arises from the spectral changes $\Delta\varepsilon_{\lambda,\kappa}$ upon formation of complex κ which is treated as a (optionally shared) local parameter. Custom normalization of this data in various ways can be accommodated. One can consider the form of Eq. S8 also for the analysis of circular dichroism data, if ε is reinterpreted to the component molar ellipticity and $\Delta\varepsilon_{\lambda,\kappa}$ a change in ellipticity caused by conformational changes upon formation of complex κ.

Fluorescence anisotropy

Steady-state anisotropy isotherms take a form of a weighted sum analogous to weighted-average sedimentation coefficients Eq. S5,

$$f_{e,i} = \frac{\sum_X \varepsilon_{\lambda,X} c_{X,free,i} \Theta_{X,free} + \sum_\kappa \left(\Delta\varepsilon_{\lambda,\kappa} + \sum_X \nu_{\kappa,X} \varepsilon_{\lambda,X} \right) c_\kappa(\{c_{Xtot,i}\}) \Theta_\kappa}{\sum_X \varepsilon_{\lambda,X} c_{X,free,i} + \sum_\kappa \left(\Delta\varepsilon_{\lambda,\kappa} + \sum_X \nu_{\kappa,X} \varepsilon_{\lambda,X} \right) c_\kappa(\{c_{Xtot,i}\})} \qquad \text{(Eq. S9)}$$

replacing sedimentation coefficients by species anisotropy values Θ, but also accounting for spectral changes $\Delta\varepsilon_{\lambda,\kappa}$ for formation of complex κ (equivalent to a *q*-factor)[13].

If extrinsic fluorescent labels are required, competition experiments can be used to study the competitive interaction between labeled and unlabeled binding partners. In contrast to the flow configuration of the SPR-SC experiment where the equilibrium mixture between soluble unmodified SBTI and CT is continuously re-supplied such that we measure the free CT in the reaction between free SBTI and CT, for the fluorescence competition experiment we have one fixed reaction volume where competitive equilibria between free SBTI and labeled SBTI for CT are established. Therefore, the experimental data from the competition experiment can be treated rigorously as a three component system, where the unlabeled material has $\varepsilon_{\lambda,X} = 0$. In the context of GMMA, for all other experiments the concentration of the labeled component are constant zero.

Dynamic light scattering

Dynamic light scattering models are part of SEDPHAT, although not used in the study of the experimental model system. Models for autocorrelation data in DLS are based on autocorrelation functions of the individual species. For example, for the field autocorrelation functions this leads to a linear superposition of species autocorrelation functions

$$f_{e.i} = g^{(1)}(\tau_i) = A_e \left[\sum_K {M_X}^2 c_{X,free}\, e^{-q^2 D_X \tau} + \sum_\kappa \left(\sum_X \nu_{\kappa,X} M_X \right)^2 c_\kappa\, e^{-q^2 D_\kappa \tau} \right] + b_e \quad \text{(Eq. S10)}$$

, each term weighted by the species' relative scattering intensity given by the species molecular weight (in the approximation that all components have the same refractive index increment). *A* represents a normalization constant related to the number of coherence areas observed, *q* the wave vector $(4\pi n_0/\lambda)sin(\vartheta/2)$ with the solvent refractive index n_0, and *D* the translational diffusion coefficient, which can be calculated from the species buoyant molar mass and sedimentation coefficient with the Svedberg equation [14]. It should be noted that in conjunction with SV-AUC data informing on sedimentation coefficients and known species molecular weights the exponents of the decay terms can be effectively constrained. Species concentrations are calculated based on mass action law Eq. S3 given known total concentrations $\{c_{Xtot,i}\}$. Alternatively to Eq. S10, intensity autocorrelation data $g^{(2)}-1$ can be modeled on the basis of Eq. S10 with as $(g^{(1)})^2$. [15] Local adjustable parameters are the baseline b_e and the amplitude A_e.

Supplementary References

(1) Schuck, P. *Ann. Rev. Biophys. Biomol. Struct.* **1997**, *26*, 541–566.

(2) Houtman, J. C. D.; Brown, P. H.; Bowden, B.; Yamaguchi, H.; Appella, E.; Samelson, L. E.; Schuck, P. *Protein Sci.* **2007**, *16*, 30–42.

(3) Dam, J.; Velikovsky, C. A.; Mariuzza, R.; Urbanke, C.; Schuck, P. *Biophys. J.* **2005**, *89*, 619–634.

(4) Brautigam, C. A. *Methods* **2011**, *54*, 4–15.

(5) Zhao, H.; Balbo, A.; Brown, P. H.; Schuck, P. *Methods* **2011**, *54*, 16–30.

(6) Schuck, P. *Anal. Biochem.* **2003**, *320*, 104–124.

(7) Harding, S. E.; Johnson, P. *The Biochemical journal* **1985**, *231*, 543–7.

(8) Batchelor, G. K. *J. Fluid. Mech.* **1972**, *52*, 245–268.

(9) Schuck, P. *Biophys. J.* **2010**, *98*, 2005–2013.

(10) Ghirlando, R. *Methods* **2011**, *54*, 145–56.

(11) Vistica, J.; Dam, J.; Balbo, A.; Yikilmaz, E.; Mariuzza, R. A.; Rouault, T. A.; Schuck, P. *Anal. Biochem.* **2004**, *326*, 234–256.

(12) Zhao, H.; Brautigam, C. A.; Ghirlando, R.; Schuck, P. *Curr. Protoc. Protein Sci.* **2012**, *in press*.

(13) Eftink, M. R. *Methods Enzymol.* **1997**, *278*, 221–57.

(14) Svedberg, T.; Fahraeus, R. *J. Am. Chem. Soc.* **1926**, *48*, 430–438.

(15) Berne, B. J.; Pecora, R. *Dynamic Light Scattering*; Dover Publications: Mineola, New York, 2000.